Analyst

PAPER

View Article Online
View Journal | View Issue

Cite this: *Analyst*, 2016, **141**, 1822

Label-free fluorescent catalytic biosensor for highly sensitive and selective detection of the ferrous ion in water samples using a layered molybdenum disulfide nanozyme coupled with an advanced chemometric model†

Jie Hu,[a] Qianfen Zhuang,[a] Yong Wang*[a] and Yongnian Ni*[a,b]

Received 30th November 2015,
Accepted 19th January 2016

DOI: 10.1039/c5an02457a

www.rsc.org/analyst

In this work, we developed a novel layered molybdenum disulfide (MoS_2) nanosheet peroxidase mimetic-based fluorescent catalytic biosensor for the sensitive and selective detection of Fe^{2+}. It was found that Fe^{2+} remarkably enhanced the catalytic activity of the MoS_2 nanosheet for oxidation of OPD to form a highly fluorescent substance, 2,3-diaminophenazine (DAPN), and the MoS_2/OPD/H_2O_2 biosensor displayed substantial fluorescence enhancement after addition of Fe^{2+} in a concentration-dependent manner. The fluorescence intensity was proportional to the concentration of Fe^{2+} over a range of 0.005–0.20 μM with a limit of detection of 3.5 nM (signal/noise = 3). When compared with the OPD/H_2O_2 biosensor, the MoS_2/OPD/H_2O_2 biosensor provided a higher sensitivity and selectivity for Fe^{2+}, suggesting the validity of the use of the MoS_2 nanosheets. To further demonstrate the feasibility of the MoS_2/OPD/H_2O_2 biosensor for Fe^{2+} detection in real water samples, we measured the three-dimensional excitation–emission spectra of the real system, and submitted the excitation–emission matrix (EEM) data to an advanced chemometrics model based on parallel factor analysis (PARAFAC). The results showed that the use of the PARAFAC model could further enhance the selectivity of the biosensor and determine Fe^{2+} concentration in the presence of unexpected interferents from real water samples. This work opens up new opportunities for the use of the catalytic properties of the MoS_2 nanosheets and advanced chemometrics models in the field of biosensors.

Introduction

The (re)discovery of graphene in 2004 by Novoselov and Geim has given impetus to the investigation of other inorganic graphene-like two-dimensional materials.[1,2] Owing to a thickness reduction to single or few layers, these graphene-analogous materials possess a wealth of unusual and fascinating physicochemical properties, and provide fundamental applications in novel nanodevices.[1,2] Among the graphene-analogous materials, a surge of intense research interest over the last few years has focused on layered transition metal dichalcogenides (TMDs), notably molybdenum disulfide (MoS_2).[3] Until now, layered MoS_2 nanosheets have provided many potential applications in optoelectronic devices,[4,5] energy storage devices,[6,7] and electrocatalysis.[8,9] More recently, layered MoS_2 nanosheets have been discovered to exhibit an intrinsic peroxidase-like activity, and have been used to fabricate various colorimetric nanozyme biosensors for the detection of H_2O_2 and some substrates.[10–14] However, the study of its application as a mimetic enzyme of peroxidase in the area of biosensing remains far from fully developed. For example, fluorescent catalytic biosensors have been recently considered to be well-suited for detection of trace levels of catalytic species because they combine the high selectivity of catalysts with the significant advantages of fluorescence techniques, such as inherent high sensitivity, simplicity, rapid action, and low cost.[15–18] However, to the best of our knowledge, almost no work has currently reported the development of fluorescent catalytic biosensors using layered MoS_2 nanosheets as a nanozyme to detect catalysts.

[a]*College of Chemistry, Nanchang University, Nanchang, Jiangxi 330031, China. E-mail: wangyong@ncu.edu.cn, ynni@ncu.edu.cn; Fax: +86 791 83969500; Tel: +86 791 83969500*

[b]*State Key Laboratory of Food Science and Technology, Nanchang University, Nanchang 330047, China*

†Electronic supplementary information (ESI) available. See DOI: 10.1039/c5an02457a

In this paper, as a proof of concept, the ferrous ion (Fe^{2+}) was selected as a model catalyst to be determined. It was reported that the iron ion is ubiquitous throughout the universe, and has wide uses in agriculture and industry.[19,20] The element plays an essential role in many environmental processes.[19,20] Accordingly, approaches for simple and rapid detection of the ferrous ion in environmental samples, especially water samples are of considerable significance. It is well known that the mixture of Fe^{2+} catalyst and hydrogen perioxide (H_2O_2) can degrade most of the reducing organic compounds.[21] Among them, *o*-phenylenediamine (OPD) can be oxidized to a highly fluorescent substance, 2,3-diaminophenazine (DAPN), in the presence of Fe^{2+} catalyst and H_2O_2.[22–25]

At the same time, the MoS_2 nanosheet synthesized hydrothermally using sodium molybdate and thiourea as the starting materials was herein found to have peroxidase-like activity, and also catalyze the oxidation of OPD by H_2O_2 to produce the highly fluorescent compound. Further addition of the ferrous ion (Fe^{2+}) to the MoS_2/OPD/H_2O_2 biosensory system can give rise to the remarkable increase in the fluorescence intensity and catalytic activity compared with that of the MoS_2 nanosheet or Fe^{2+} alone. Therefore, the phenomenon of the synergism of the MoS_2 nanosheet and Fe^{2+} as cocatalysts was exploited to construct a label-free "turn on" fluorescent catalytic biosensor for the detection of Fe^{2+}. Moreover, it is worth noting that the selectivity of most fluorescent biosensors fabricated at present is not sufficient for quantitative determination of an analyte of interest in natural samples, such as the presently studied environmental water samples, although fluorescent biosensors display high selectivity.[26–30] This is predominantly because traditional fluorescent biosensors cannot effectively deal with the natural interferents causing a matrix effect or/and unknown fluorescent constituents in real samples without a thorough previous physical and chemical separation procedure, and frequently, the fluorescent spectra of the investigated analyte inevitably overlaps with that of the natural interferents in real samples.[26,27] Fortunately, a good solution to the problem of the natural interferents in real samples is to apply the trilinear three-way fluorescence excitation–emission matrix (EEM) data combined with second-order calibration methods based on parallel factor analysis (PARAFAC).[26,27] The approach can achieve the so-called second-order advantage, which allows for the analysis of samples with a complex background, permitting accurate quantification of an analyte of interest even in the presence of unsuspected interferents.[28] The outstanding property of this approach exploits mathematical means to avoid the requirement of interferent elimination with concomitant savings in analysis time and the use of harmful organic solvents, which conform well to the principles of green chemistry. Therefore, to enhance the applicability of the Fe^{2+} biosensor in real water samples, we herein collected the three-way EEM data of the MoS_2/OPD/H_2O_2 biosensory system, and processed them with the PARAFAC algorithm to realize an accurate determination of Fe^{2+} in the presence of unexpected interferents from environmental water samples.

Experimental

Reagents and chemicals

Hydrogen peroxide (H_2O_2), *o*-phenylenediamine (OPD), and acetic acid were purchased from Sinopharm Chemical Reagent Co., Ltd (Shanghai, China). Sodium molybdate dihydrate ($Na_2MoO_4{\cdot}2H_2O$) was purchased from Tianjin Chemical Reagent 4th Factory Kaida Chemical Plant (Tianjin, China). Thiourea was bought from Tianjin Chemical Reagent 4th Factory Fengchuan Chemical Plant (Tianjin, China). Sodium acetate trihydrate was purchased from Xilong Chemical Reagent Co., Ltd (Shantou, China). The acetate buffer (200 mM, pH = 4.5) for detection was made up using sodium acetate and acetic acid. Unless specifically noted, all reagents were of analytical reagent grade and used as received. Ultrapure water was used in all experiments.

Instrumentation and software

Transmission electron microscopy (TEM) characterizations and TEM-based selected area electron diffraction (SAED) measurements were performed using a JEM-2010 microscope (JEOL Co., Japan) operated at an accelerating voltage of 200 kV. Atomic force microscope (AFM) images were obtained using an AJ-III Instrument (Shanghai Aijian Nanotechnology, China) in the tapping mode. All fluorescence spectral measurements were performed using a Perkin Elmer LS-55 photoluminescence spectrometer (PerkinElmer Co., USA) with a standard 10 mm path length cell. The classical fluorescence spectra were measured at the excitation wavelength of 410 nm in the emission range of 370–680 nm every 0.5 nm at a scanning rate of 1500 nm min^{-1}. The excitation–emission matrix (EEMs) were recorded at the excitation wavelengths between 320 and 550 nm (every 10 nm), and at different excitation wavelengths between 370 nm and 680 nm (every 0.5 nm). All excitation and emission slitwidths were set to be 10 nm, and the scan speed was set at 1500 nm min^{-1}. The employed PARAFAC algorithm was implemented using the codes provided by Bro,[31] which can be freely downloaded from http://www.models.kvl.dk/algorithms. The Rayleigh and Raman scattering from the EEMs, uncorrelated with the analyte, can be quickly and effectively removed using the smooth method provided by earlier literature.[32] All the calculations were performed in MATLAB environment on a Core 2 Duo microcomputer.

Synthesis of MoS_2 nanosheets

The typical synthesis of the MoS_2 nanosheets was carried out as below: 2.2 g of $Na_2MoO_4{\cdot}2H_2O$ and 2.0 g of thiourea were dissolved in 70 mL of ultrapure water under magnetic stirring. The pH value of such a solution was then adjusted to less than 1 by the addition of 12 M hydrochloric acid. The resultant solution was then transferred into a 100 mL Teflon-lined stainless steel autoclave and heated at 200 °C for 24 h. Subsequently, the autoclave was allowed to cool to room temperature naturally. The obtained samples were centrifuged at 6000 rpm and washed with water and absolute ethanol

several times, and finally dried in a vacuum oven overnight at 60 °C.

General procedure of fluorescent biosensing of Fe^{2+}

Into a 5 mL plastic test tube, 10 μL of luminescent MoS_2 nanosheets (0.1 mg mL^{-1}), appropriate volumes (x μL) of Fe^{2+} standard solutions, and selected volumes of (1370–x μL) water were micropipetted directly and mixed thoroughly. Then, 100 μL of OPD (10 mM) and 500 μL of acetate buffer (200 mM, pH = 4.5), and 20 μL of H_2O_2 (10 mM) were added to give a final volume of 2.00 mL, and the solution was mixed thoroughly. After the solution was equilibrated for 30 min, the resultant solution was transferred into a 3.5 mL quartz cell. The fluorescence spectrum was measured with respect to water. All the analysis herein was performed at room temperature.

Theoretical background for PARAFAC model

The PARAFAC theory is well documented in the literature[31] and therefore a brief description is herein provided. The excitation–emission matrix (EEM) fluorescence on J emission wavelengths and K excitation wavelengths for I samples can give a three-way data array $\boldsymbol{X}_{I\times J\times K}$. This data array possesses an internally mathematical structure described as trilinear, and is thus decomposed by the trilinear PARAFAC model as below:

$$x_{ijk} = \sum_{n=1}^{N} a_{in} b_{jn} c_{kn} + e_{ijk} (i = 1,\ 2, \ldots, I;\ j = 1,\ 2, \ldots, J;\ k = 1,\ 2, \ldots, K) \quad (1)$$

where x_{ijk} denotes the input fluorescence intensity for sample i, emission wavelength j, and excitation wavelength k, and N represents the number of components, which is regarded as the total number of fluorescent species consisting of the analyte of interest and the background as well as unknown interferents. b_{jn} and c_{kn} are the normalized intensities at the emission wavelength j and the excitation wavelength k, and a_{in} is the relative concentration of component n in the i-th sample. The column vectors a_n, b_n, and c_n can be respectively collected to form the corresponding relative concentration matrix $\boldsymbol{A}_{I\times N}$, emission spectral matrix $\boldsymbol{B}_{J\times N}$, and excitation spectral matrix $\boldsymbol{C}_{K\times N}$. The term e_{ijk} is the element of the three-way residual data array $\boldsymbol{E}_{I\times J\times K}$.

The advantage of this technique is that the solution of the PARAFAC model is unique, constituting the basis of the so-called second-order advantage. The model is initialized with the loadings providing the best fit after some trials runs, chosen from the comparison of the results given by generalized rank annihilation and several orthogonal random loadings.[33] To ensure that the final solution was chemically meaningful, some constraints like non-negativity and/or unimodality of the spectral and concentration profiles, and orthogonality between the spectral matrix and concentration matrix are often used.[31] The number of components can be estimated using the core consistency diagnostic (CORCONDIA) test and/or through visual inspection of the spectral profiles.[34]

Results and discussion

Characterization of layered MoS_2 nanoflare

Fig. 1A displays a typical TEM image of the synthesized MoS_2 sample. As can be clearly seen from Fig. 1A, the MoS_2 sample possessed a sheet-like structure. Looking at the inset in Fig. 1A, it can be seen that the selected area electron diffraction (SAED) of the MoS_2 sample presented two hexagonal rings, composed of clear diffraction points, which arose from the specific crystal orientations of MoS_2. The two rings were respectively located at the 0.27 nm and 0.16 nm lattice distances, corresponding to the (100) and (110) lattice planes of MoS_2.[35] The AFM image of the MoS_2 sample is depicted in Fig. 1B, wherein the thickness of the MoS_2 sample is estimated to be 0.7–1.5 nm, corresponding to 1–2 monolayers of MoS_2. The crystalline structure of the MoS_2 sample was further investigated through X-ray diffraction (XRD). The diffraction peaks at 2θ = 14.4°, 2θ = 33.5° and 2θ = 58.0°, in Fig. 1C can be respectively indexed to the (002), (l00), and (110) crystalline planes of the MoS_2 (ICDD, reference number, 77-1716).

Fluorescence behaviour of synergistically enhanced biosensor for Fe^{2+}

The peroxidase-like activity of the as-prepared MoS_2 nanosheets was tested for the oxidation of OPD in the presence of H_2O_2. Fig. 2 shows that upon the addition of MoS_2 to the OPD/H_2O_2 solution, a maximum emission peak at 550 nm with excitation at 410 nm could be clearly observed. This fluorescent maxima at 550/410 nm was assigned to the oxidation product, 2,3-diaminophenazine (DAPN), of OPD.[22–25] And the fluorescent spectral band of the MoS_2/OPD/H_2O_2 system was more intense than that of the OPD/H_2O_2 system (blank),

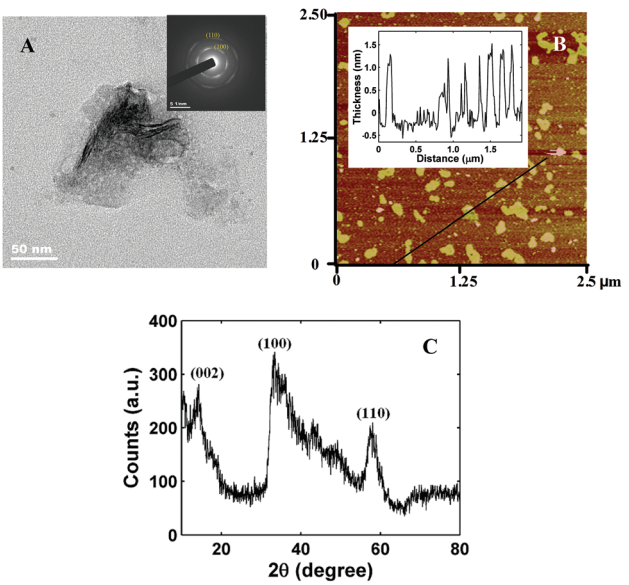

Fig. 1 Characterizations of the MoS_2 nanosheets. (A) TEM image, inset: the related selected area electron diffraction; (B) AFM image, inset: the corresponding section analysis; (C) XRD pattern.

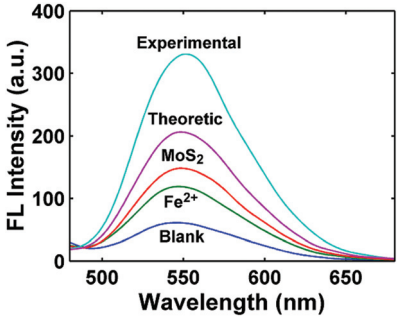

Fig. 2 Fluorescence spectra for the OPD/H_2O_2 system (blank), the MoS_2/OPD/H_2O_2 system, the Fe^{2+}/OPD/H_2O_2 system, as well as the theoretical and experimental spectra of the MoS_2/OPD/H_2O_2 system and the Fe^{2+}/OPD/H_2O_2. The theoretical spectrum of the MoS_2/OPD/H_2O_2 system and the Fe^{2+}/OPD/H_2O_2 system can be achieved by subtracting the spectrum of the blank from the spectrum of the MoS_2/OPD/H_2O_2 system plus the spectrum of the Fe^{2+}/OPD/H_2O_2 system. Conditions: Fe^{2+}, 0.10 μM; MoS_2, 1.0 μg mL^{-1}; OPD, 0.5 mM; H_2O_2, 0.1 mM; pH, 4.5, reaction time, 30 min.

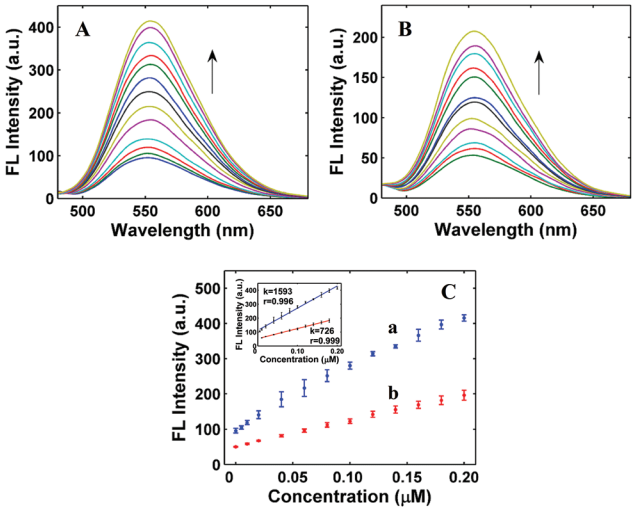

Fig. 3 Fluorescence spectra for the MoS_2/OPD/H_2O_2 biosensory system (A) and the Fe^{2+} OPD/H_2O_2 biosensory system (B) with different Fe^{2+} concentrations (0, 0.005, 0.01, 0.02, 0.04, ..., 0.20 μM). (C) Dependence of the fluorescence intensity at 550 nm on the Fe^{2+} concentration for the MoS_2/OPD/H_2O_2 system (a) and the Fe^{2+} OPD/H_2O_2 system (b). Inset: the related calibration curve for Fe^{2+} detection.

indicating that the as-prepared MoS_2 nanosheets possessed an intrinsic peroxidase-like activity. Moreover, we can notice from Fig. 2 that the Fe^{2+} ion can catalytically oxidize OPD in the presence of H_2O_2 to produce the fluorescent DAPN, which was in good agreement with the previous literature.[22–25] More importantly, it was found from the data shown in Fig. 2 that upon the addition of Fe^{2+} to the OPD/H_2O_2 solution in the presence of the MoS_2 nanosheets, the fluorescent spectral band of the Fe^{2+}/MoS_2/OPD/H_2O_2 system was noticeably enhanced, and was far greater than that its theoretical one. Correspondingly, we performed the experiments on the colorimetric response of the systems under the same conditions (Fig. S1†). The results depicted in Fig. S1† were in good agreement with those obtained from the fluorescent responses. All these suggested the synergistic influence of the MoS_2 nanosheets on Fe^{2+} catalysis, and the observation can be used to fabricate a sensitive biosensor for Fe^{2+} detection.

MoS_2 nanosheets for improved sensitivity and selectivity of biosensor for Fe^{2+}

Because the MoS_2 nanosheets can remarkably enhance Fe^{2+} catalysis, we herein constructed a biosensor for detection of Fe^{2+} using the MoS_2 nanosheets. The effect of different variables on the reaction and fluorescence intensity was studied, including OPD concentration (0–800 μM), H_2O_2 concentration (0–180 μM), MoS_2 concentration (0–7.0 μg mL^{-1}), and reaction time (0–60 min). On the basis of higher sensitivity, we selected 500 μM of OPD, 100 μM of H_2O_2, and 0.5 μg mL^{-1} of MoS_2. In addition, we found that when the reaction time reached 30 min, the fluorescence intensity almost reached the highest value. Hence, we chose 30 min as the optimal reaction time. Under the optimum experimental conditions, several calibration solutions with different concentrations (0–0.20 μM) of Fe^{2+} were prepared, and the related fluorescent spectral data were measured (Fig. 3A). It was observed from Fig. 3A and C that as the Fe^{2+} concentration increased, the fluorescence intensity strengthened. The inset in Fig. 3C depicts a calibration graph which was obtained as a function of Fe^{2+} concentration over the 0.005–0.20 μM range. The calibration equation for the MoS_2/OPD/H_2O_2 biosensory system was F = 1593 $c_{Fe^{2+}}$ + 112 (r = 0.996), and the limit of detection (LOD) was 3.5 nM at a signal-to-noise ratio of 3, which was far less than the maximum level (5.36 μM) of Fe^{2+} in drinking water set by the World Health Organization.[36] For comparison, we collected the fluorescence spectral data of the OPD/H_2O_2 solution with different concentrations of Fe^{2+} under the same experimental conditions (Fig. 3B). It was found that the fluorescence intensity was linear with the Fe^{2+} concentration in the 0.01–0.18 μM range (inset in Fig. 3C: LOD = 8.8 nM, r = 0.999). The regression equation for the OPD/H_2O_2 biosensory system was F = 726 $c_{Fe^{2+}}$ + 53. In the light of the above-mentioned sensitivity and LOD value, a conclusion can be drawn that the MoS_2/OPD/H_2O_2 biosensory system for detection of Fe^{2+} was more sensitive than the OPD/H_2O_2 biosensory system. The result implied that the MoS_2 nanosheets facilitate the enhancement of the sensitivity of the Fe^{2+} biosensor.

To investigate the selectivity of the aforementioned biosensory systems for Fe^{2+} detection, control experiments were carried out using seventeen kinds of metal ions including Fe^{2+}, Fe^{3+}, Ag^{+}, Al^{3+}, Ba^{2+}, Ca^{2+}, Cd^{2+}, Co^{2+}, Cr^{3+}, Cu^{2+}, Hg^{2+}, K^{+}, Mg^{2+}, Mn^{2+}, Na^{+}, Ni^{2+}, Pb^{2+} or Zn^{2+} at a concentration of 0.20 μM. The fluorescence spectra of the two biosensory systems without (blank) or with each metal ion are displayed in Fig. 4A and B. The corresponding selectivity plot is shown in Fig. 4C and D, and the results were represented as normalized spectral intensities (($F_{metal} - F_{blank}$)/($F_{Fe^{2+}} - F_{blank}$)), where F_{metal} was the fluorescence intensity with each metal ion, $F_{Fe^{2+}}$

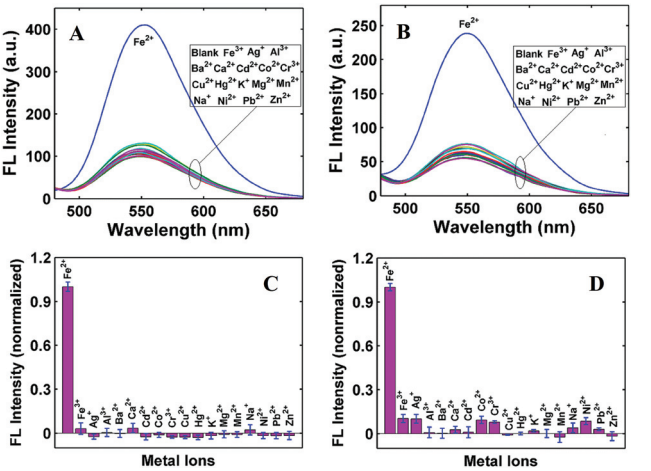

Fig. 4 Fluorescence spectra for the MoS_2/OPD/H_2O_2 biosensory system (A) and the Fe^{2+}/OPD/H_2O_2 biosensory system (B) with different individual metal ions (concentration = 0.20 μM). Selectivity of the MoS_2/OPD/H_2O_2 biosensory system (C) and the Fe^{2+}/OPD/H_2O_2 biosensory system (D) for detection of Fe^{2+}.

was the fluorescence intensity with Fe^{2+}, and F_{blank} denoted the fluorescence intensity without each metal ion. It is clearly observed in Fig. 4C and D that compared with the OPD/H_2O_2 biosensory system, the MoS_2/OPD/H_2O_2 biosensory system displayed higher selectivity for Fe^{2+}, indicating that the MoS_2 nanosheets facilitate the improvement of the selectivity of the Fe^{2+} biosensor. More importantly, five metal ions (Ba^{2+}, Ca^{2+}, K^+, Mg^{2+}, Na^+) often exist in fairly large quantities in lake water, and thus we further assessed the selectivity of the MoS_2/OPD/H_2O_2 biosensory system for Fe^{2+} determination using the five metal ions at a concentration far greater than that of Fe^{2+} (Fig. S2†). As can be seen from Fig. S2,† Fe^{2+} even at a very low concentration (10 nM) still had an observable fluorescence signal, which was remarkably greater than those of Ba^{2+}, Ca^{2+}, K^+, Mg^{2+} or Na^+ at a high concentration (0.1 mM or 1 mM). The results implied that these metal ions most likely did not interfere with the determination of Fe^{2+} in lake water.

PARAFAC analysis for the MoS_2/OPD/H_2O_2 biosensory system

Because the use of the MoS_2 nanosheets can increase the sensitivity and selectivity of the Fe^{2+} biosensor, we herein performed PARAFAC analysis only for the MoS_2/OPD/H_2O_2 biosensory system. The three-dimensional fluorescence excitation–emission spectra for thirteen samples containing Fe^{2+} over the 0–0.20 μM concentration range were recorded at the excitation wavelengths between 320 and 550 nm (every 10 nm), and at different excitation wavelengths between 370 nm and 680 nm (every 0.5 nm), which constructed a three-way sample-fluorescence emission–fluorescence excitation data array of size 13 × 621 × 16. Fig. 5A and Fig. S3A–3M† show the contour map of the fluorescence excitation–emission matrix (EEM) data. From these figures, we can observe the presence of both Rayleigh and Raman scatterings. These scatterings did not contain any information concerning the fluorescence properties of the analyte, and thus did not conform to a trilinear structure, which complicated the correct decomposition of the profile of each mode using second-order PARAFAC methods. To avoid the effect of nonlinear signals, we treated scatterings using the earlier proposed interpolation method[32] in the area affected by Rayleigh and Raman scatterings (Fig. 5B shows a representative EEM spectra as a contour map after removing the scatterings).

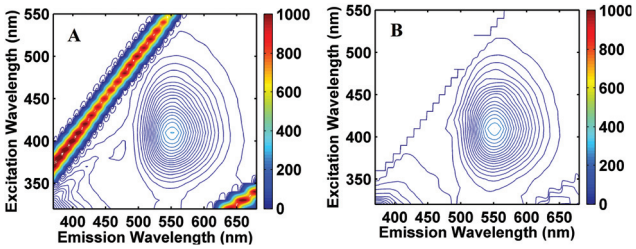

Fig. 5 (A) Contour map of the fluorescence excitation–emission matrix data for the MoS_2/OPD/H_2O_2 biosensory system in the presence of 0.1 μM Fe^{2+}. (B) The corresponding contour map after removing the scatterings.

Fig. 6 depicts the resolved normalized emission and excitation spectra, and relative concentration profiles of two components present in thirteen calibration samples obtained by decomposition of the EEM spectra using the two-component PARAFAC model. It was clearly observed from Fig. 6A and B that the pair of excitation/emission wavelengths related to the maximum fluorescent intensity of the first component (blue line) was approximately 410 nm/550 nm, corresponding to the oxidation product DAPN of OPD. And the excitation and emission spectra of the second component (green line), which possibly originated from the background (fluorescent OPD and/or some impurities of the reagents used), overlapped with those of the first component, DAPN (Fig. 6A and B). Moreover,

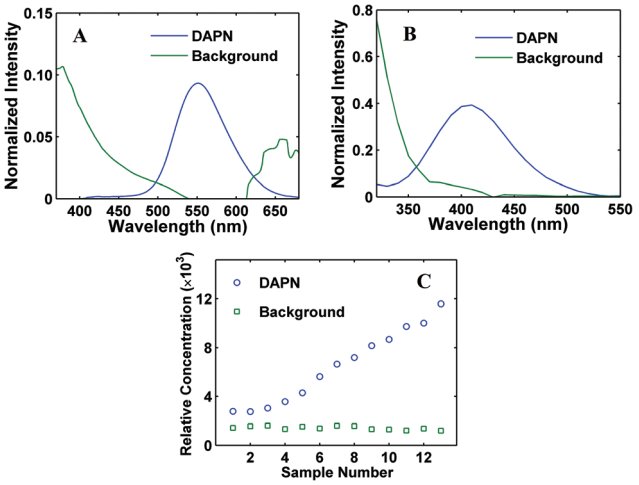

Fig. 6 Resolved normalized emission (A) and excitation (B) spectra, and relative concentration profiles (C) of two components present in the calibration samples using the two-component PARAFAC model.

it was found from Fig. 6A that there were unexpected small peaks in the emission spectrum of the background, which likely arose from the unmodeled scatterings.[37] As seen from Fig. 6C, the recovered relative concentrations of DAPN in the sample mode followed the expected pattern that the concentrations of DAPN increased with the increase of Fe^{2+} concentrations. The linear classical univariate regression of the decomposed relative concentration (c_{DAPN}) can be performed against real concentrations of Fe^{2+} ($c_{Fe}2+$: 0.005–0.20 μM). The regression equation was c_{DAPN} = 43 466 $c_{Fe}2+$ (μM) + 2738 with the correlation coefficient of 0.996. The resolved relative concentrations of the background in Fig. 6C were maintained at a constant level, suggesting that these samples had an almost identical background. All the results clearly confirmed that PARAFAC modelling can improve the understanding of the MoS_2/OPD/H_2O_2 biosensory system.

Analysis of water samples with PARAFAC model

To further demonstrate the feasibility and reliability of our proposed method, we applied the MoS_2/OPD/H_2O_2 biosensory system coupled with the PARAFAC model to detect Fe^{2+} in real water samples. The water samples were collected from Longten Lake (Nanchang, Jiangxi, China). The samples were first filtered with a 0.22 μm membrane, and then centrifuged for 30 min at 12 000 rpm. The obtained samples and the four standard addition samples with Fe^{2+} at different concentrations were analyzed in triplicate using the proposed method. The EEM spectral data of these water samples were collected, and their contour maps are displayed in Fig. S4A–4E.† It is clearly found from Fig. S4A–4E† that the shape of the contour map for these water samples was very different from that for the aforementioned calibration samples, implying the presence of interferent in the water samples. Then, the EEM spectral data were prepossessed with an interpolation method to remove the effect of scatterings. Subsequently, PARAFAC was applied to the treated three-way data arrays built by joining the above-mentioned calibration data matrices with those of the water samples. Following the same procedure in the PARAFAC analysis described previously, we found that the number of components to be included in the PARAFAC model was three, which was likely assigned to DAPN, a background, and an unexpected component from the water samples matrix.

Fig. 7 illustrates the normalized emission and excitation spectra, as well as the relative concentrations decomposed by PARAFAC. It was noticed from Fig. 7A and B that the excitation/emission peaks corresponding to the first component (blue line) were 410 nm/550 nm, which were the spectral characteristics of DAPN. The second component had an emission and excitation spectra similar to the aforementioned background. And the third component had excitation and emission maxima at 429.5 nm and 330 nm, and the component were attributed to humic-like components from the water samples matrix.[38] Looking at the emission and excitation spectra of the three components, it was found that the spectra of DAPN overlapped with those of the other two components,

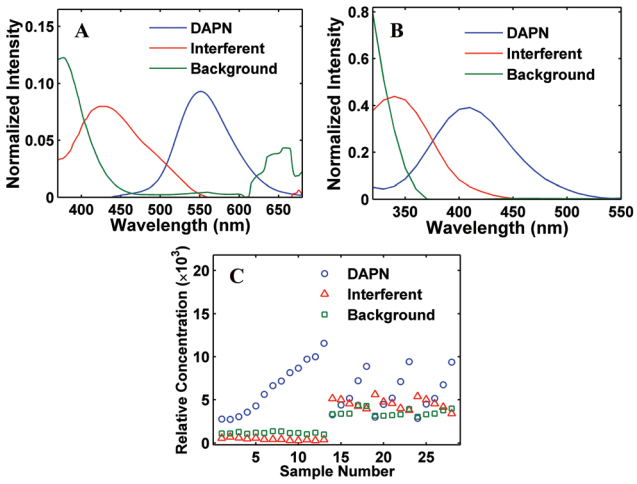

Fig. 7 Normalized emission (A) and excitation (B) spectra as well as the relative concentrations (C), which were recovered from fluorescence EEM data of the calibration samples and water samples decomposed by the PARAFAC model with three components.

suggesting that it was difficult for the accurate and sensitive quantitation of the analyte of interest in the presence of unexpected background and interferents using the direct fluorimetric method without the aid of the PARAFAC model. Fig. 7C shows that due to the complexity of water samples, the water samples possessed far more background and interferent than those calibration samples, and the relative concentrations of the background and interferent from water samples were almost not influenced by the addition of Fe^{2+}, implying little interaction of Fe^{2+} with the background and interferent. At the same time, we can note that Fe^{2+} concentrations were positively correlated with the relative concentrations of DAPN. The relative concentrations of DAPN resolved from the calibration samples and the added concentration of Fe^{2+} can be used to construct a calibration equation. The calibration equation was c_{DAPN} = 43 446 $c_{Fe}2+$ (μM) + 2727 with the correlation coefficient of 0.996. It is worth noting that the slope value of the equation was very close to that value of 43 466 without water samples, demonstrating the feasibility and reliability of successful detection of Fe^{2+} in the presence of unexpected background and interferent with the aid of a PARAFAC model.

Table S1† summarizes the analytical results for the detection of Fe^{2+} in water samples using the developed method and the standard method based on the preconcentration of Fe^{2+} and the 1,10-phenanthroline assay.[39] As shown in Table S1,† the determined concentrations of Fe^{2+} by the proposed method agreed well with those given by the standard method. The mean recoveries of Fe^{2+} detected by the proposed method reached to 92–110% with the coefficient of variation (CV) of 2.5–6.1%. These good results suggested that the established approach can overcome the problem of the presence of unsuspected background and interferents in real samples, and thus further increased the selectivity of the fabricated MoS_2/OPD/H_2O_2 biosensor for Fe^{2+}.

Conclusions

In summary, the layered MoS_2 nanoflares synthesized by the hydrothermal method can catalyze H_2O_2 oxidizing *o*-phenylenediamine (OPD) substrate to produce a highly fluorescent substance, 2,3-diaminophenazine (DAPN), demonstrating that the MoS_2 nanosheets can act as peroxidase mimetics. The catalytic activity of the MoS_2 nanosheets in the presence of Fe^{2+} was far higher than the MoS_2 nanosheets alone. Therefore, using the OPD/H_2O_2 catalyzed fluorescence reaction, the MoS_2 nanosheets were exploited as a new type of fluorescent catalytic biosensor for detection of Fe^{2+}. Moreover, it was found that the use of the MoS_2 nanosheets can increase the sensitivity and selectivity of the fluorescent catalytic biosensor. The developed MoS_2/OPD/H_2O_2 biosensing platform exhibited sensitive and selective detection of Fe^{2+} with a linear range from 0.005 to 0.20 μM and with a detection limit of 3.5 nM. To effectively deal with the natural interferents from matrix effect or/and unknown fluorescent components in real water samples, we employed the fluorescence EEM data of the biosensing system together with an advanced chemometrics model based on PARAFAC to realize the accurate quantification of Fe^{2+} in the presence of unknown interferents from water samples. This work opens a new door for the use of the catalytic properties of the MoS_2 nanosheets and advanced chemometrics approaches in the field of biosensors.

Acknowledgements

This work was supported by the National Natural Science Foundation of China (NSFC-21305061), the Natural Science Foundation of Jiangxi Province (20151BAB213014 and 20151BAB203021), the State Key Laboratory of Chemo/Biosensing and Chemometrics of Hunan University (SKLCBC-2013010), and the State Key Laboratory of Food Science and Technology of Nanchang University (SKLF-ZZA-201302 and SKLF-ZZB-201303).

References

1 K. S. Novoselov, A. K. Geim, S. V. Morozov, D. Jiang, Y. Zhang, S. V. Dubonos, I. V. Grigorieva and A. A. Firsov, *Science*, 2004, **306**, 666–669.
2 M. S. Xu, T. Liang, M. M. Shi and H. Z. Chen, *Chem. Rev.*, 2013, **113**, 3766–3798.
3 R. Lv, J. A. Robinson, R. E. Schaak, D. Sun, Y. F. Sun, T. E. Mallouk and M. Terrones, *Acc. Chem. Res.*, 2015, **48**, 56–64.
4 D. Lembke, S. Bertolazzi and A. Kis, *Acc. Chem. Res.*, 2015, **48**, 100–110.
5 T. P. Nguyen, Q. V. Le, K. S. Choi, J. H. Oh, Y. G. Kim, S. M. Lee, S. T. Chang, Y. H. Cho, S. Choi, T. Y. Kim and S. Y. Kim, *Sci. Adv. Mater.*, 2015, **7**, 700–705.
6 T. Stephenson, Z. Li, B. Olsen and D. Mitlin, *Energy Environ. Sci.*, 2014, **7**, 209–131.
7 X. Tong, E. Ashalley, F. Lin, H. D. Li and Z. M. M. Wang, *Micro Nano Lett.*, 2015, **7**, 203–218.
8 Y. Shi, J. Wang, C. Wang, T. T. Zhai, W. J. Bao, J. J. Xu, X. H. Xia and H. Y. Chen, *J. Am. Chem. Soc.*, 2015, **137**, 7365–7370.
9 H. Y. Song, Y. N. Ni and S. Kokot, *Biosens. Bioelectron.*, 2014, **56**, 137–143.
10 X. R. Guo, Y. Wang, F. Y. Wu, Y. N. Ni and S. Kokot, *Analyst*, 2015, **140**, 1119–1126.
11 T. R. Lin, L. S. Zhong, L. Q. Guo, F. F. Fu and G. N. Chen, *Nanoscale*, 2014, **6**, 11856–11862.
12 N. R. Nirala, S. Pandey, A. Bansal, V. K. Singh, B. Mukherjee, P. S. Saxena and A. Srivastava, *Biosens. Bioelectron.*, 2015, **74**, 207–213.
13 Z. Sun, Q. S. Zhao, G. H. Zhang, Y. Li, G. L. Zhang, F. B. Zhang and X. B. Fan, *RSC Adv.*, 2015, **5**, 10352–10357.
14 K. Zhao, W. Gu, S. S. Zheng, C. L. Zhang and Y. Z. Xian, *Talanta*, 2015, **141**, 47–52.
15 T. Fu, X. H. Zhao, H. R. Bai, Z. L. Zhao, R. Hu, R. M. Kong, X. B. Zhang, W. H. Tan and R. Q. Yu, *Chem. Commun.*, 2013, **49**, 6644–6646.
16 J. W. Liu and Y. Lu, Fluorescent DNAzyme Biosensors for Metal Ions Based on Catalytic Molecular Beacons, in *Methods in Molecular Biology*, ed. V. V. Didenko, Humana Press Inc., New Jersey, 2006.
17 G. Orellana, D. Garcia-Fresnadillo and M. C. Moreno-Bondi, *Afinidad*, 2007, **64**, 257–264.
18 M. W. Tsang, P. K. So, S. Y. Liu, C. W. Tsang, P. H. Chan, K. Y. Wong and Y. C. Leung, *Biotechnol. J.*, 2015, **10**, 126–135.
19 K. H. Nealson and D. Saffarini, *Annu. Rev. Microbiol.*, 1994, **48**, 311–343.
20 J. P. Pestaner, K. G. Ishak, F. G. Mullick and J. A. Centeno, *Biol. Trace Elem. Res.*, 1999, **69**, 191–198.
21 C. Walling, *J. Chem. Soc.*, 1975, **8**, 125–131.
22 D. B. Galadilovich and K. P. Stolyarov, *J. Anal. Chem. USSR*, 1983, **38**, 666–670.
23 V. M. Mekler and S. M. Bystryak, *Anal. Chim. Acta*, 1992, **264**, 359–363.
24 P. J. Tarcha, C. P. Chu and D. Whittern, *Anal. Biochem.*, 1987, **165**, 230–233.
25 K. Zaitsu and Y. Ohkura, *Anal. Biochem.*, 1980, **109**, 109–113.
26 S. A. Bortolato, J. A. Arancibia and G. M. Escandar, *Anal. Chem.*, 2008, **80**, 8276–8286.
27 A. F. T. Moore, H. C. Goicoechea, F. Barbosa and A. D. Campiglia, *Anal. Chem.*, 2015, **87**, 5232–5239.
28 A. C. Olivieri, *Anal. Chem.*, 2005, **77**, 4936–4946.
29 A. M. D. L. Pena, N. M. Diez, M. C. M. Garcia, D. B. G. Gil and F. Canada–Canada, *Talanta*, 2007, **73**, 304–313.
30 G. N. Piccirilli and G. M. Escandar, *Analyst*, 2010, **135**, 1299–1308.
31 R. Bro, *Chemom. Intell. Lab. Syst.*, 1997, **38**, 149–171.

32 K. R. Murphy, C. A. Stedmon, D. Graeber and R. Bro, *Anal. Methods*, 2013, **5**, 6557–6566.
33 P. C. Damiani, I. Duran Meras, A. Garcia Reiriz, A. Jimenez Jiron, M. de la Pena and A. C. Olivieri, *Anal. Chem.*, 2007, **79**, 6949–6958.
34 J. A. Porini and G. M. Escandar, *Anal. Methods*, 2011, **3**, 1494–1500.
35 L. P. Hansen, Q. M. Ramasse, C. Kisielowski, M. Brorson, E. Johnson, H. Topsoe and S. Helveg, *Angew. Chem., Int. Ed.*, 2011, **50**, 10153–10156.
36 WHO, *Guidelines for Drinking–Water Quality*, WHO Press, Geneva, 2011.
37 Y. Li, H. L. Wu, Y. J. Yu, S. R. Zhang, Y. Chen, D. Z. Tu, C. C. Nie, H. Xu and R. Q. Yu, *Anal. Methods*, 2012, **4**, 3987–3996.
38 K. R. Murphy, C. A. Stedmon, P. Wenig and R. Bro, *Anal. Methods*, 2014, **6**, 658–661.
39 GB/T 5750.6-2006, *Standard Examination Methods for Drinking Water–Metal Parameters*, Standardization Administration of the People's Republic of China, 2006.